

(Un)predictability of strong El Niño events

John Guckenheimer¹, Axel Timmermann², Henk Dijkstra³, and Andrew Roberts⁴

¹Mathematics Department, Cornell University, Ithaca, NY 14853

²IBS Center for Climate Physics, Pusan National University, Busan, South Korea

³Institute for Marine and Atmospheric Research Utrecht, Department of Physics and Astronomy, Utrecht University, Utrecht, The Netherlands

⁴Cerner Corporation, Kansas City, Missouri

May 9, 2019

Abstract

The El Niño-Southern Oscillation (ENSO) is a mode of interannual variability in the coupled equatorial Pacific coupled atmosphere/ocean system. El Niño describes a state in which sea surface temperatures in the eastern Pacific increase and upwelling of colder, deep waters diminishes. El Niño events typically peak in boreal winter, but their strength varies irregularly on decadal time scales. There were exceptionally strong El Niño events in 1982-83, 1997-98 and 2015-16 that affected weather on a global scale. Widely publicized forecasts in 2014 predicted that the 2015-16 event would occur a year earlier. Predicting the strength of El Niño is a matter of practical concern due to its effects on hydroclimate and agriculture around the world. This paper discusses the frequency and regularity of strong El Niño events in the context of chaotic dynamical systems. We discover a mechanism that limits their predictability in a conceptual “recharge oscillator” model of ENSO. Weak seasonal forcing or noise in this model can induce irregular switching between an oscillatory state that has strong El Niño events and a chaotic state that lacks strong events. In this regime, the timing of strong El Niño events on decadal time scales is unpredictable.

1 Introduction

The problem in predicting El Niño events is that they occur quite irregularly, and their development seems to be different each time [20]. In addition to observations, the amplitudes of El Niño events in a long simulation of the GFDL CM2.1 coupled ocean-atmosphere General Circulation model with constant forcing are highly variable on decadal time scales [31]. The predictability horizon of individual El Niño events is thought to be about 6-9 months, depending on the season and the phase of the ENSO cycle. During boreal spring the coupled ocean-atmosphere system is thought to be at its frailest state [30]. Then the system is most susceptible to perturbations [29] which leads to a ‘spring’ predictability barrier in April/May [18]. The role of the initial error pattern has been emphasized and in particular its interaction with the seasonal cycle and the internal ENSO cycle [21, 8, 34]. However, since detailed surface and ocean subsurface observations of ENSO began in the 1950s, very strong El Niño events have occurred only once every 15-20 years (1982, 1997 and 2015) and the processes controlling their predictability horizon are largely unknown.

Similar to investigations of tipping points [24], we would like to identify precursors that predict the strength of impending events and their frequency on both shorter and longer time scales. Processes determining ENSO variability and its limits of predictability have been studied in conceptual models [25, 28, 16]. Such models seek to identify key dynamical processes in the complex, coupled ocean-atmosphere system in the tropical Pacific.

This paper discovers a new dynamical mechanism that limits the predictability of strong El Niño events in the low-dimensional conceptual Jin-Timmermann (JT) model of ENSO originally proposed by Jin [16] and then extended by Timmermann et al. [27]. The state space variables of this deterministic model are sea

surface temperatures of the equatorial western Pacific and eastern Pacific, and the thermocline depth (e.g. the depth of the 20°C isotherm) of the western Pacific. Nonlinear terms in the model are associated with the wind-induced anomalous advection of sea surface temperature anomalies and thermocline dynamics that affect these state variables. Comparisons of this reduced order model with observational data confirm that the model embodies the basic features of ENSO in the tropical Pacific [1].

Recently, a multiple time scale analysis of the JT model was performed to gain new insight into its dynamics [22]. This work transformed the model equations into an equivalent dimensionless system whose equations are

$$\begin{cases} x' &= \rho\delta(x^2 - ax) + x(x + y + c - c \tanh(x + z)) \\ y' &= -\rho\delta(ay + x^2) \\ z' &= \delta(k - z - \frac{x}{2}), \end{cases} \quad (1)$$

The variables x, y and z of this model represent the sea surface temperature difference between the eastern and western equatorial Pacific, the sea surface temperature of the western equatorial Pacific relative to a nominal reference temperature, and the thermocline depth of the western Pacific, respectively. Each of the five parameters δ, ρ, c, k and a represents a combination of physical characteristics of the tropical Pacific. The tuning of these parameters and the sensitivity of the El Niño variability to these parameters is discussed in [22]. Before we present additional analysis of this model, we recall relevant background material from dynamical systems theory.

2 Sensitive Dependence to Initial Conditions and Predictability

Strong El Niño events are typically characterized by a threshold of average sea surface temperature anomaly in the eastern equatorial Pacific, e.g., the Niño 3.4 region (5N-5S, 170W-120W). [2] Within the setting of the JT model, we set the threshold $x > -1.5$ for strong El Niño events since x represents the difference in sea surface temperature of the eastern and western tropical Pacific. The events are then *recurrences* to the phase space region $x > -1.5$. Predictability of strong El Niño events in the JT model is then a matter of the frequency and regularity of recurrences to this region. We use a simple discrete time dynamical system to illustrate the type of unpredictability that we subsequently find in the JT model.

Sensitive Dependence to Initial Conditions [23] has been a key concept in the study of chaotic dynamical systems: pairs of nearby initial conditions yield trajectories that separate from each other. Statistical theories of chaotic attractors [33] emphasize asymptotic properties like invariant measures, Lyapunov exponents and entropies. There are dynamical systems in which multiple time scales are an emergent phenomenon. Some trajectories spend long times near metastable invariant sets, occasionally making transitions between them. We use the term *epoch* to denote a maximal time interval when the system is close to one of the metastable invariant sets.

Our viewpoint is strongly influenced by the Wentzell-Freidlin theory of stochastically perturbed dynamical systems [10]. Imagine a deterministic dynamical system with several attractors and a small stochastic or random perturbation of this system. Wentzell and Freidlin introduce a Markov chain whose states are the attractors of the deterministic system with transition probabilities given by the observed frequencies of transitions between their basins of attractions in trajectories of the stochastic system. This same Markov model can be used for deterministic systems which have an attractor comprised of several *almost invariant* sets with infrequent transitions from one to another [11].

We illustrate these concepts with iterations of the one dimensional map $g(x) = \alpha*x(1-x^2)$, $x \in [-\infty, \infty]$. When $2 < \alpha < 3\sqrt{3}/2 \approx 2.598$, this map has two attractors in the intervals $[-1, 0]$ and $[0, 1]$. At $\alpha = 1/\sqrt{3}$, the two attractors merge. Iterations of one dimensional maps are an intricate subject with deep mathematical structure. [5]. For some values of the parameter α , g will have stable periodic orbit(s) that are its attractors, but for a positive measure set of α , the map has chaotic attractor(s). Figure 1 illustrates the dynamics when $\alpha = 2.6$, seemingly a value that gives rise to a single chaotic attractor. The intervals $[g(-1/\sqrt{3}), 0]$ and $[0, g(1/\sqrt{3})]$ are almost invariant: trajectories spend quite long periods of time in these intervals before switching to the other interval. This is shown in Figure 1c where a trajectory segment of length 1000 is plotted. There are epochs between mode switches of quite different lengths in this subplot. Figure 1d shows a histogram (on a log scale) of the number of epochs of different lengths in a trajectory of 10^6 iterates. The

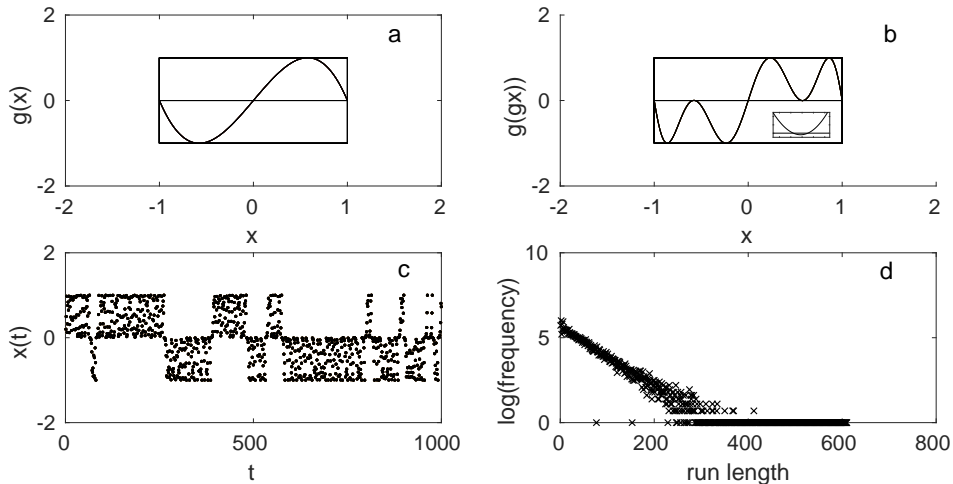


Figure 1: Mode switching in a discrete one dimensional iteration: (a) Graph of the function $g(x) = 2.6 * x(1 - x^2)$. The intervals $[g(-1/\sqrt{3}), 0]$ and $[0, g(1/\sqrt{3})]$ are almost invariant, but short subintervals near $\pm 1/\sqrt{3}$ map to the opposite interval. (b) The second iterate of g together with an expanded plot near $1/\sqrt{3}$ showing that the local minimum of the map is negative. (c) 1000 iterates beginning at $x = 0.2$. Epochs in which the sign of the iterates remain constant are clearly visible. (d) $\log(\text{number of epochs of length } n)$ against n in a trajectory segment of 10^6 iterates.

longest epoch has length 610; the shortest has length 8. The approximately linear slope of the graph suggests that the epoch lengths can be modeled by a Poisson distribution. In a longer trajectory of 10^7 iterates, we find that *all* pairs of integers (m, n) with $8 \leq m, n \leq 60$ occur as successive epoch lengths, indicating that the length of an epoch does not enable one to predict the length of the next epoch. Superficially, successive epoch lengths seem to be statistically independent of each other.

The unpredictability of epoch lengths in this model is related to its sensitive dependence to initial conditions. Nearby initial conditions yield trajectories that separate from one another so that information about their approximate location is lost after a moderate number of iterates. In this example, recurrences to the intervals $[-\infty, -1]$ and $[1, \infty]$ mark the transitions from one basin to the opposite one. The set of initial conditions where a transition occurs at the n^{th} iterate is a finite union of intervals, but the number of intervals increases geometrically with n and, for a positive measure set of α , their distribution approaches an absolutely continuous invariant measure [5].

We also computed the epoch lengths for sample trajectories of the stochastic map $g_r(x) = 2.595 * x(1 - x^2) + 0.005 * \xi$ (where ξ is a normally distributed random variable) to reside in one of the two attractor basins. Here, we are certain that the dynamics have an absolutely continuous invariant measure and exponential decay of correlations [3]. The resulting distribution of epoch lengths has no apparent differences from those shown in Figure 1(d) for the deterministic system with two almost invariant sets. Both the deterministic and random versions of this model have epoch lengths that are unpredictable from past history.

3 Two Attractors of the JT Model

Several different types of attractors are found in the JT model. We are especially interested in those that have strong El Niño events. Since the variable x represents the difference in sea surface temperatures between the eastern and western tropical Pacific, these events are marked by small values of $|x|$. We used bifurcation analysis in our search for different types of attractors. The program MATCONT [7] was used to locate points of Hopf bifurcation [14] and then to identify points of “generalized Hopf” bifurcations where the bifurcation is neither subcritical nor supercritical. Starting at parameters with a supercritical Hopf bifurcation and varying parameter δ , periodic orbits were continued until they lost stability at a period doubling bifurcation

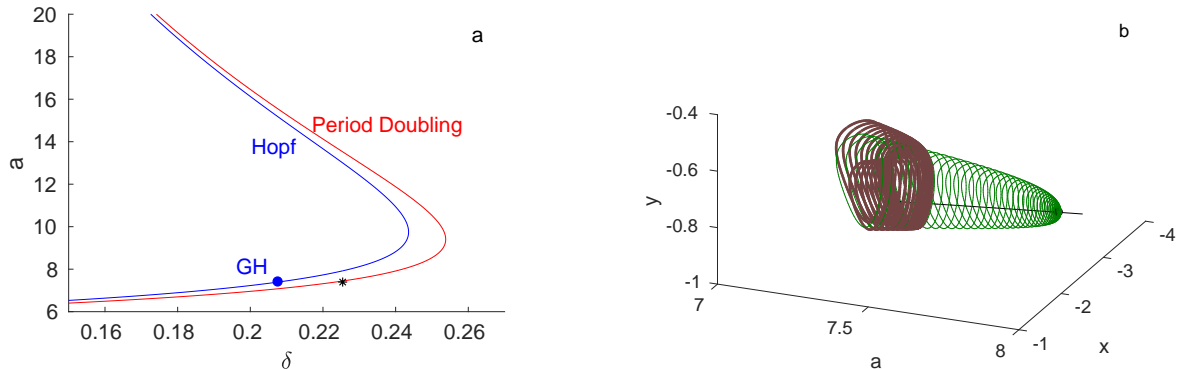


Figure 2: (a) (Blue) Hopf bifurcation and (red) period doubling curves in the (δ, a) plane. The point near $(7.3945, 0.2077)$ labelled GH separates subcritical and supercritical bifurcations [7] along the Hopf curve. The black asterisk shows the (δ, a) parameter values $(7.3939, 0.225423)$ studied extensively in this paper. These values are below the period doubling curve. The parameters $[\rho, c, k] = [0.3224, 2.3952, 0.4032]$ (b) A bifurcation diagram with varying parameter a showing a curve of equilibria (black) that passes through a Hopf bifurcation point (black dot) near $\delta = 7.9224$, the (green) family of periodic orbits emerging from the Hopf point and the (brown) family of “doubled” periodic orbits emerging from a period doubling bifurcation near $\delta = 7.4438$. The parameters $[\delta, \rho, c, k] = [0.225423, 0.3224, 2.3952, 0.4032]$

and then went through a period doubling cascade to a chaotic attractor [9]. Figure 2 displays results of these MATCONT calculations. Further increases in δ led to a regime with an MMO attractor. Decreasing δ showed that the ranges of δ with MMO and chaotic attractors overlapped. At the end of this section, we discuss the bifurcations that occur on the boundaries of the overlap region.

The parameters

$$[\delta, \rho, c, k, a] = [0.225423, 0.3224, 2.3952, 0.4032, 7.3939]$$

in the overlap region are used here to study bistability and mode switching in the JT model. Figure 3 shows two trajectories of the model with these parameter values. The blue trajectory appears to be a periodic mixed mode oscillation (MMO) with period approximately 12.1 years and a single intense El Niño event each period that follows a series of growing fast (sub-annual) oscillations. We show below that this trajectory is more complicated with small variations from one cycle to the next. The time scales in these dynamics are slightly shorter than those seen in observations of ENSO, but our purpose here is to describe a new fundamental mechanism that could potentially limit the predictability of strong El Niño events rather than finding an optimal quantitative fit of this highly reduced model to data. The red trajectory is chaotic with oscillations whose amplitude variation is smaller than those of the MMO.

A central feature of the MMO cycle is an equilibrium point that is a saddle focus: the MMO approaches the equilibrium along its one dimensional stable manifold and then spirals away, following its two dimensional unstable manifold. The number of oscillations within the MMO cycle and their minimum amplitude depends upon how close it approaches the equilibrium. The growing amplitude oscillations of the MMO cycle terminate in a strong El Niño event during which the sea surface temperatures of eastern and western tropical Pacific become almost the same. This El Niño is followed rapidly by a La Niña event in which the system “recharges” [16], reestablishing higher sea surface temperatures and thermocline depth in the western than eastern Pacific. The recharged system flows back toward the equilibrium where the cycle repeats.

The chaotic attractor resembles those found in many other three dimensional vector fields. In contrast to strong El Niño events, x remains far from 0. As illustrated in Figure 4, this attractor can be analyzed by introducing a cross-section and studying its return map. Figure 4a shows the intersection of a trajectory with the cross-section $x = x_{eq}$, where $x_{eq} \approx -2.4839$ is the value of x at the equilibrium point. Black filled circles in the figure are intersections of a periodic orbit with the cross-section. This periodic orbit appears to be on the boundary of the basin of attraction of the attractor, and it plays a central role in bifurcations of the attractor. The return map contracts in one direction, and stretches and folds in a second direction. Figure 4b shows the folding by plotting the value of z at each return to the cross-section against the value

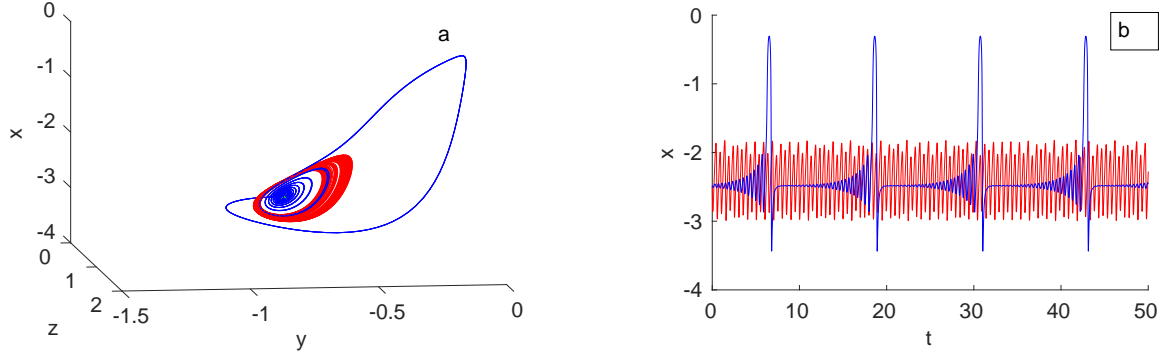


Figure 3: (a) Phase portraits of a chaotic attractor (red) and an MMO periodic orbit (blue) that coexist at parameters $[\delta, \rho, c, k, a] = [0.225423, 0.3224, 2.3952, 0.4032, 7.3939]$. The equilibrium point is a partially obscured blue dot. (b) Time series of the x coordinate of the two trajectories.

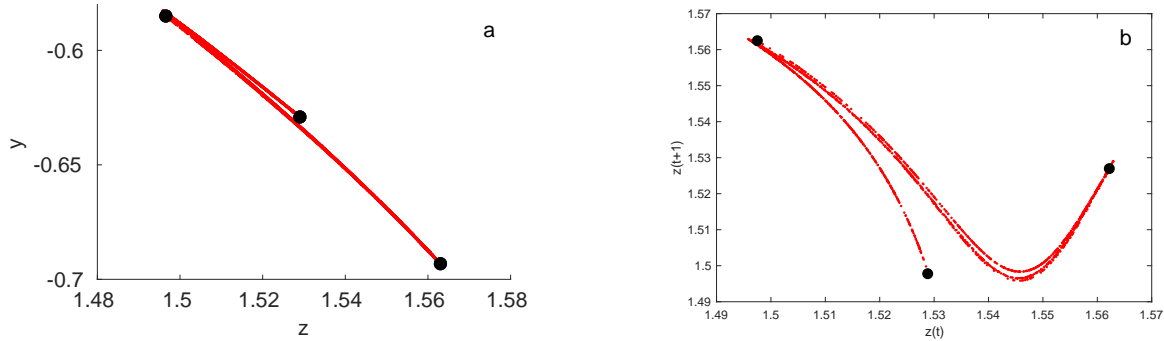


Figure 4: (a) Intersections (y_n, z_n) of a trajectory in the chaotic attractor with the plane $x = x_{eq} \approx -2.4839$. Black dots show intersections of a periodic orbit lying on the basin boundary with the cross-section. (b) z_{n+1} against z_n for this trajectory.

of z at the previous return. There is sensitivity to initial conditions within the chaotic attractor, but it is relatively mild: nearby initial conditions separate along the attractor without leaving it.

The basins of attraction of the two attractors are intertwined with each other in an intricate way, as illustrated in Figure 5. Trajectories starting in a 500×500 initial condition grid in the cross-section $x = x_{eq} \approx -2.4839$ were computed. The figure colors those initial conditions that approach the chaotic attractor yellow and those that approach the MMO attractor blue. Intersections of the chaotic attractor with the cross-section are plotted red and the intersections of the MMO attractor with the cross-section are plotted blue. The attractors appear to have fractal basin boundaries [13]. Further evidence for this assertion was obtained by computing a saddle periodic orbit Γ with negative Floquet multipliers in the basin boundary. Were the basin boundary smooth, Γ would separate its unstable manifold into two pieces, one consisting of trajectories that approach the MMO attractor and one consisting of trajectories that approach the chaotic attractor. However, a trajectory with initial condition on one side of the unstable manifold returns on the opposite side because the multipliers are negative. Consequently, the local unstable manifold of Γ is a one sided, non-orientable Möbius strip that cannot constitute the common boundary of two different attractor basins. Instead, the two basins of attraction interleaved thin layers and each approaches Γ from both sides of its stable manifold. Thus, there are large sets in which it is difficult to predict which basin a chosen initial condition will belong to. Both attractors are very close to their basin boundaries, so carefully chosen perturbations of very small magnitude can induce trajectories to flow from the chaotic to the MMO attractor and vice versa. To explore mode switching in this model, we investigated regions where nearby trajectories separate quickly.

Figure 6 visualizes the rapid separation of trajectories. Figure 6a shows a collection of 100 trajectory

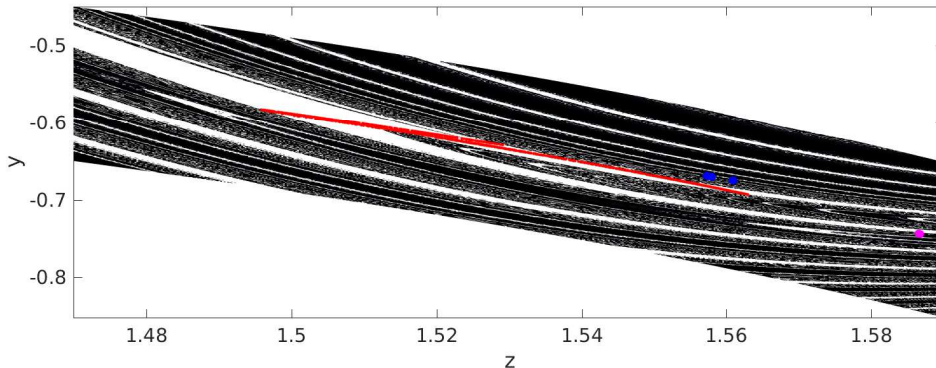


Figure 5: The colored region is a 500x500 grid that straddles the intersection of the chaotic attractor with the cross-section $x = x_{eq} \approx -2.8439$. Points are colored by whether their Trajectories of light colored points approach the chaotic attractor while trajectories of dark colored points approach the MMO attractor. The red markers and blue dots mark intersections of the chaotic attractor and MMO with the cross-section, respectively. The (overlapping) magenta markers locate initial points for the trajectories displayed in Figure 6a.

segments with initial conditions in the cross-section $x = x_{eq}$. These initial conditions were chosen along a curve of length approximately 0.0005 whose image under the third iterate of the return map appears to stretch between the two attractors. Figure 6b shows the y coordinate for the third return of points in a region W similar to the region displayed in Figure 5. In the middle of this strip, there is a “ridge” of points for which the y coordinate of the return is close to -0.1 . These are points whose third return is associated with a strong El Niño event. The sides of the ridge are points where the third iterate of the return map has large stretching. This can be quantified by computing the finite time Lyapunov exponent or FTLE [15] of trajectories in W . The FTLE is the largest singular value of the variational equations of the flow map along a trajectory segment of specified length. It measures the maximal stretching of infinitesimally close trajectories along the trajectory segment. Figure 7 plots this quantity on a log scale in a strip of initial conditions in the plane $x = -2.4839$ and trajectory segments of time length $\log_{10} 0.7 \approx 5$. Values are on a base 10 log scale. The center of the strip, indicated by its blue color, consists of points in the MMO basin of attraction and their FTLEs are approximately 5. Trajectory segments along two flanking strips have FTLE two orders of magnitude larger, demonstrating the high sensitivity to initial conditions there.

These properties contrast with the one dimensional map g discussed in the previous section. As the parameter a of that example increases to its critical value $3\sqrt{3}/2$, the basins of two attractors touch at a single point and the two attractors merge into one. In the JT model, bifurcations of the MMO and chaotic attractors occur at different parameter values and the two attractors do not merge to become one. Apparently, when one of the invariant sets ceases to be an attractor, most points that were in its basin of attraction have trajectories that now flow to the other attractor. We investigated how this happens as the parameter a is varied.

In the case of the chaotic attractor of the JT model, a *boundary crisis bifurcation* [12] occurs where the attractor becomes a non-attracting invariant set. As a decreases to a value close to 7.3938587 the periodic orbit on the basin boundary displayed in Figure 4 approaches the attractor. For smaller values of a , a chaotic invariant set persists, but it is no longer attracting. Trajectories can “escape” from the former attractor basin along the unstable manifold of the periodic orbit.

The bifurcations associated with the MMO attractors also involve a boundary crisis. The MMO attractor for $a = 7.3939$ comes close to the equilibrium point which is a saddle focus with eigenvalues approximately -1.46 and $0.127 \pm 4.47i$. Because the ratio of the negative eigenvalue to the real part of the complex eigenvalues has large magnitude, a large volume of phase space is drawn toward the stable manifold of the equilibrium before their trajectories spiral away slowly along the two dimensional unstable manifold of the equilibrium. Moreover, trajectories starting close to the equilibrium in the unstable manifold increase their distance from it by a factor of only about 1.2 per revolution as determined by the ratio of the real and imaginary parts

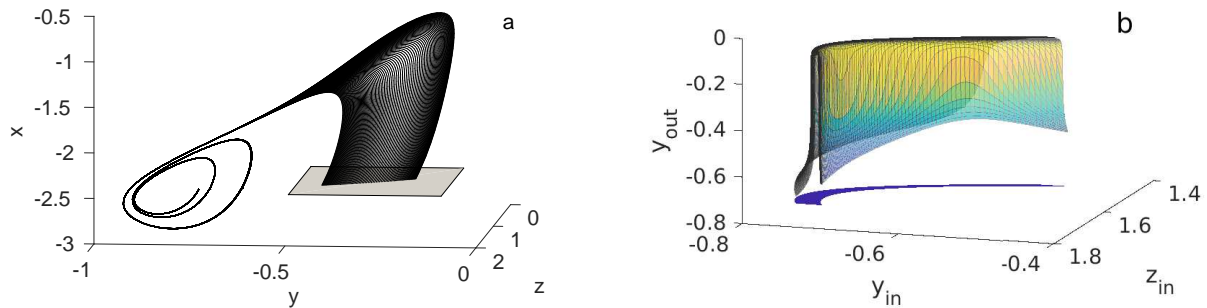


Figure 6: (a): Ensemble of 100 trajectory segments in the cross section $x = x_{eq} \approx -2.4839$ are plotted to their third return to this cross-section, drawn gray. Initial conditions lie along a curve of length approximately 0.0005. The final points of the segments lie on a curve of length larger than 0.4. (b): The image of the y -coordinate under the third iterate of the return map of a thin strip of initial conditions (dark blue) of width 0.035 in the cross section $x = x_{eq}$. Points in the middle of the strip make a large amplitude excursion representing a strong El Niño. The map stretches the y -coordinate by a factor of order 10^3 where the returns have intermediate amplitude between those on the ridge and the strip boundaries.

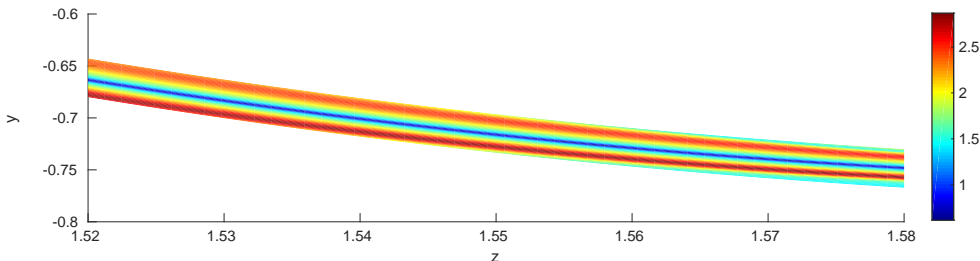


Figure 7: The largest finite time Lyapunov exponent for trajectory segments of length five. Initial conditions are a 50×50 grid in the plane $x = -2.4839$ and values of the FTLE are plotted on a base 10 log scale. Points in the middle of the strip make a large amplitude excursion representing a strong El Niño event.

of the complex eigenvalues. Nonetheless, motion along the unstable manifold has the potential to disperse trajectories through a large part of the phase space. Some of the trajectories in the unstable manifold undergo strong El Niño events and approach the MMO attractor.

We examine next a return map to the cross-section $x = -1.5$, which we set (arbitrarily) as a threshold for strong El Niño events. This value is larger than the maximum of x in the chaotic attractor (see Figure 3.) Figure 8a plots intersections of the unstable manifold of the equilibrium with this cross-section as large blue dots. There is a fold that occurs near $z = 0.835$ dividing the intersection into two branches that are close together. To investigate the next return of the unstable manifold to the cross-section, we approximate the intersection by a quadratic curve, plotted as black dots in the figure. The returns of the black points are plotted as green x's. This image lies close to the intersection of the unstable manifold of the equilibrium with the cross-section, so we regard the return map as approximately one dimensional. Figure 8b shows the graph of this one dimensional map, parametrized by the z coordinates of domain and range. There is an interval (roughly $z \in [0.835, 0.837]$) mapped into itself. A further computation using Newton's method on the return map locates a fixed point p at $(y, z) \approx (-0.07566, 0.83542)$ with one eigenvalue approximately -1.245 and the other smaller than 10^{-6} , confirming that the return map is approximately rank 1. Since the magnitude of one eigenvalue is larger than 1, the periodic orbit containing p is not stable, precluding that it is the MMO attractor. Nonetheless, the MMO attractor lies close to this periodic orbit. As the parameter a varies, the one dimensional approximations of the return map to the cross-section $z = 1.5$ undergo a “full” set of bifurcations for unimodal maps. The first bifurcation of the return map is a saddle-node bifurcation of a fixed point in the a interval $[7.3915, 7.3939]$. This bifurcation produces a stable periodic MMO with a

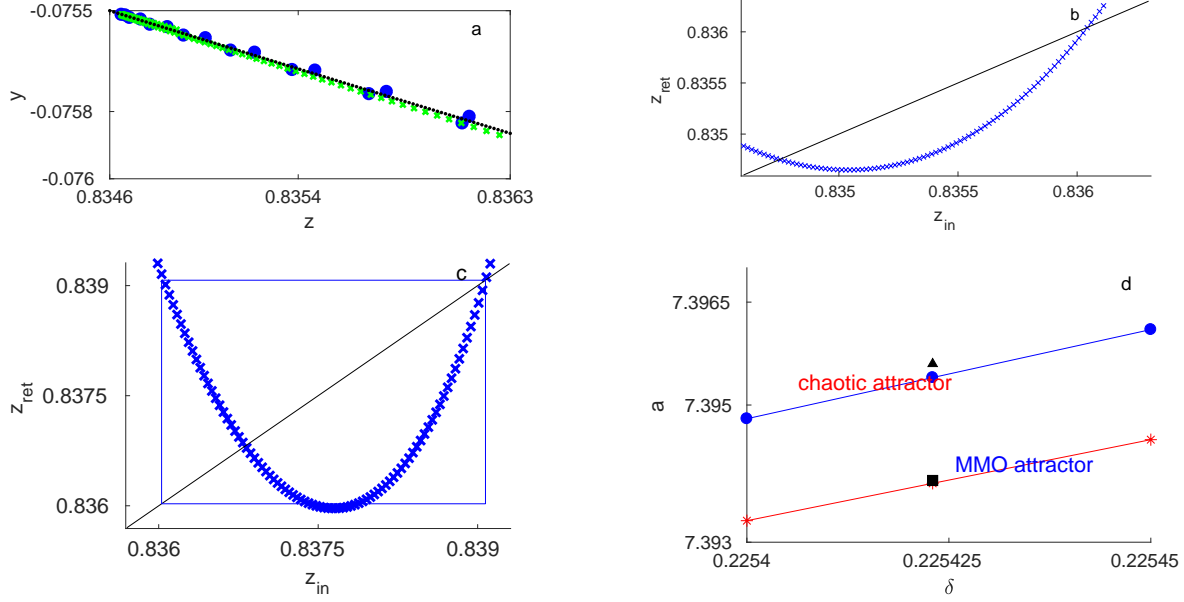


Figure 8: (a) Intersections of the unstable manifold of the equilibrium with the cross-section $x = -1.5$ are plotted as blue filled circles. A quadratic fit to these points is plotted as black dots. Images under the return map for the black points are plotted as green x's. (b) Return map values of the z -coordinate plotted against their initial values on the black curve of subplot (a). The black line is $z_{ret} = z_{in}$. The parameters $(\delta, a) = (0.225423, 7.393)$. The interval $[0.835, 0.837]$ is mapped into itself in a unimodal manner. (c) The approximate one dimensional return map for $(\delta, a) = (0.225423, 7.3956)$. Note that this return map has a non-attracting horseshoe. (d) Approximate bifurcation boundaries for the two types of attractors. Chaotic attractors are present in the region that lies above the red curve marked by asterisks. Along this curve, a periodic orbit touches the attractor in a boundary crisis. MMO attractors are present in the region below the blue curve marked by filled circles. Crossing this curve from below to above, MMO attractors become invariant sets that intersect the cross-section $x = 1.5$ in a non-attracting horseshoe. The bistability region where both types of attractors exist is the strip between the two curves. The parameters $(\delta, a) = (0.225423, 7.3939)$ inside the strip, but near the chaotic bifurcation boundary, are displayed as a black square. Figure 3 displays points of the periodic orbit that collides with the chaotic attractor in a boundary crisis. The parameters $(\delta, a) = (0.225423, 7.3956)$ outside the bistability strip are marked by a black triangle. Subplot (c) displays the non-attracting horseshoe for the return map to $x = 1.5$ for these parameters.

single strong El Niño event each cycle. This is followed by a cascade of period doubling bifurcations and chaotic MMOs as a increases [9]. At $a = 7.3956$, the return map has a horseshoe; i.e, a non-attracting invariant set topologically equivalent to a shift on two symbols [14]. This is illustrated in Figure 8c. All of these MMO attractors have only small modulations of an MMO periodic orbit and make repeated passages near the equilibrium point, producing strong El Niño events of similar frequency.

Having identified bifurcations on the boundaries of the strip of the (δ, a) parameter space where there is bistability. Values of δ were selected and then a divide and conquer strategy was utilized with varying a . In the region with chaotic attractors, the distance between the attractor chaotic attractors and the periodic orbit shown in Figure 3 indicates the distance to the bifurcation boundary. The scale of Figure 3 does not allow one to see this distance, but it is clearly visible for values of a farther from the boundary. Newton's method was applied to the return map in order to compute the periodic orbits with high precision. The extent of the attractor was determined by computing intersections of along trajectory segment with the cross-section. On crossing the bifurcation curve, we observed a discontinuous increase in the set of intersections of trajectory and cross-section. For the MMO attractors, we computed approximate return maps like those displayed in Figure 8b,c. The boundary crisis occurs where the image of the minimum value of the return map is its fixed

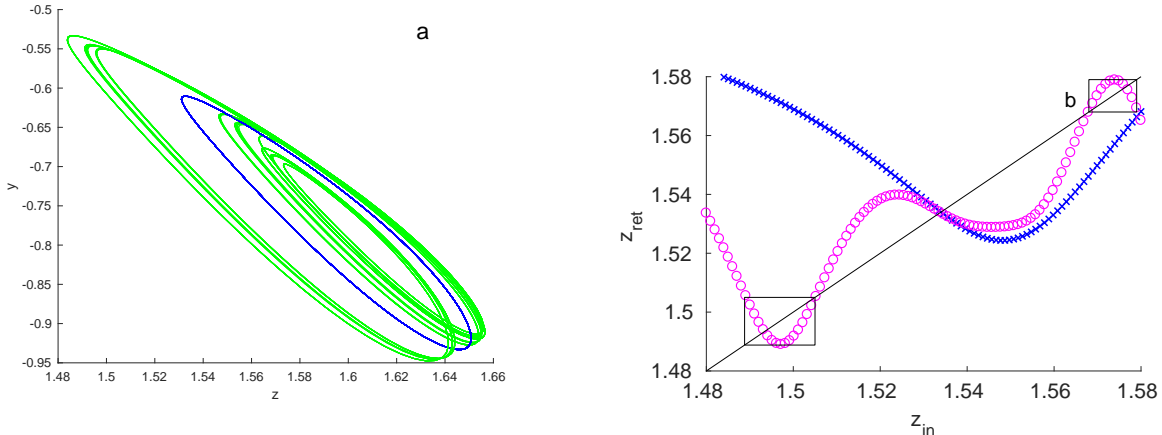


Figure 9: (a): Two trajectories for parameter value $a = 7.453$, a periodic orbit (blue) and a chaotic attractor (green). (b): Images of the z -coordinate under return maps for a curve of initial conditions that lie close to the image of the return map. Blue x's are images of the return map; magenta circles are images of the third iterate. The third iterate has subintervals (shown by black boxes) that are mapped into themselves in addition to a stable fixed point near 1.534.

point of positive slope. This is similar to the bifurcation displayed for the one dimensional map g in Section 2. In Figure 8c, the image of the minimum value is clearly larger than the fixed point, so that the map has a horseshoe. Figure 8d displays three points on each of the two bifurcation boundaries. This subplot also shows the parameter values $(\delta, a) = (0.225423, 7.3939)$ that we have studied intensively as well as the parameters $(\delta, a) = (0.225423, 7.3956)$ that lie just outside the bistability strip. These (minimal) computations show that the strip of bistability is thin but not exceedingly so. On the scale of the figure, the boundaries are close to parallel, suggesting that the strip may be quite long.

These explorations of the parameter space of the JT model only begin to probe the dynamics found in the model. There are also trajectories in the unstable manifold of the equilibrium that do not make strong El Niño excursions. The boundary between the regions that do and do not make these excursions occurs in the strips of points with large FTLE described above. We expect to find chaotic, non-attracting invariant sets in these regions. For values of $a > 7.453$, the unstable manifold of the equilibrium no longer seems to contain trajectories that have strong El Niño events, precluding the existence of MMO attractors like those we have described. This is also a situation that bears resemblance to phenomena observed in the Koper model [17]. There, MMO trajectories are observed when the unstable manifold of the equilibrium intersects a repelling slow manifold [6] of a two-time scale system with two slow variables and one fast variable. Tangency of these two manifolds locates the parameter space boundary between regions with and without MMOs. Similarly here, we observe strong El Niño events when the unstable manifold of the equilibrium intersects the strip with large FTLE. Even when there are no MMO attractors, bistability may be present. Figure 9 illustrates bistability between a periodic orbit and a chaotic attractor. These examples exhibit diverse types of ENSO dynamics in the JT model, but we do pursue them further in this paper. Our main goal is to demonstrate unpredictability where mode switching between attractors with and without strong El Niño events occurs abruptly. This is the subject of the next section.

Mode Switching

The model of Jin and Timmermann [27] includes terms representing annual forcing from the seasonal cycle of solar insolation and stochastic forcing (e.g., due to rapidly varying wind stress on the sea surface). We found that the addition of either of these components to our simulations is capable of inducing mode switching between the two attractors discussed in the previous section. Figure 10 illustrates a simulation of the periodically forced system. The parameter a was made a sinusoidally varying function of time with period one year and amplitude 0.002. Even at this small forcing amplitude, the system switches erratically

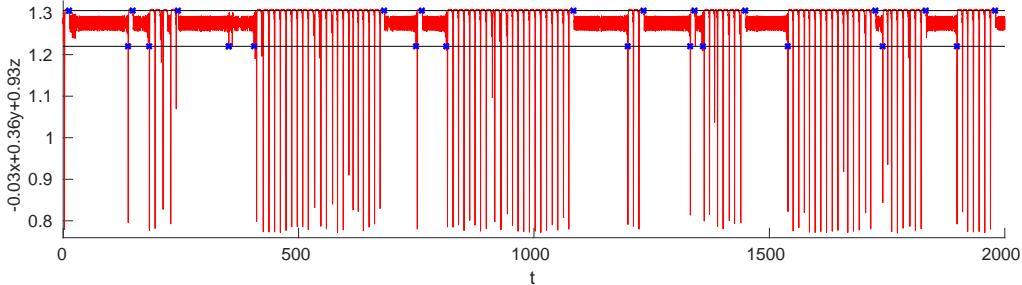


Figure 10: Time series of the function $g(x, y, z) \approx -0.0303x + 0.3600y + 0.9325z$ on a portion of a trajectory computed with $a = 7.3939 + 0.002 \sin(1.8t)$ and $[\delta, \rho, c, k] = [0.225423, 0.3224, 2.3952, 0.4032]$. The units of time are years. The crosses mark a subset of points where the trajectory crosses the thresholds $g = 1.306$ and $g = 1.22$ as described in the text. The oscillations of g lie between these thresholds during chaotic epochs.

between two almost invariant sets that approximate the attractors of the unforced model. The figure shows a representative time series of 2000 years selected from a simulation of 100,000 years. To visualize the almost invariant sets in a time series, we defined an “observable” g to be the projection onto the line orthogonal to the eigenspace of the unstable complex eigenvalues at the equilibrium point. The oscillations of g near the chaotic attractor have much smaller magnitude than those of the MMO attractor. The epochs during which the trajectory is close to one of the two attractors are readily apparent in the time series of g . The switching between modes is quite abrupt, and the duration of the epochs is irregular. We sought to investigate the distribution and independence of these durations, but found it difficult to define precise phase space boundaries to use in segmenting the trajectory into epochs automatically.

We set two thresholds for the function g and computed the times when g decreased through a threshold. The values of the thresholds were chosen to be intermediate between the range of oscillations of g in the chaotic and MMO attractors. They are plotted as black lines in Figure 10. Most of the chaotic attractor epochs lie between two successive events, with the upper threshold crossed at the beginning of the epoch and the lower threshold crossed at the end of the epoch. Moreover, the duration of most of these epochs is substantially larger than the roughly decadal duration between strong El Niño events during their epochs. This prompted us to select pairs of successive events separated by a time duration longer than 15 years as bracketing chaotic epochs. In most cases, blue crosses on the upper threshold mark the onset of chaotic epochs, while those on the lower threshold mark the termination of the epochs. The complements of these time intervals were regarded as strong El Niño epochs. In some instances, such as a time interval near $t = 20200$, there are shorter oscillations in the chaotic range that have not been identified as chaotic epochs.

Figure 11(a) displays a histogram of the number of epochs of duration less than 400 years in bins of width 10. (The longest epoch has a duration of approximately 540 years.) These durations are quite long compared to those observed in simulations of large climate models [32]. However, we chose a very small amplitude for the periodic component of a to make it easier to segment a trajectory into epochs. With larger magnitude of the periodic variation of a , the epochs are shorter and our criteria for segmenting a trajectory into epochs breaks down. The distribution of epoch durations is roughly exponential. Figure 11(b) is a scatter plot which shows pairs of successive epoch durations. Apart from higher density of shorter durations, there is no apparent pattern. We conclude that epoch durations and ENSO regime predictability in this JT model with small annual forcing are unpredictable [26].

Discussion

Reconstructions of past climate from historical data indicate that ENSO is highly variable with long periods of larger and smaller variance on decadal time scales [4, 19]. Simulations of global climate models reach similar conclusions [32]. There are many potential explanations for why ENSO is so variable. We have demonstrated here that interactions of only a few degrees of freedom in the highly reduced Jin-Timmermann model can produce unpredictability of strong El Niño events and a new type of ENSO complexity on a

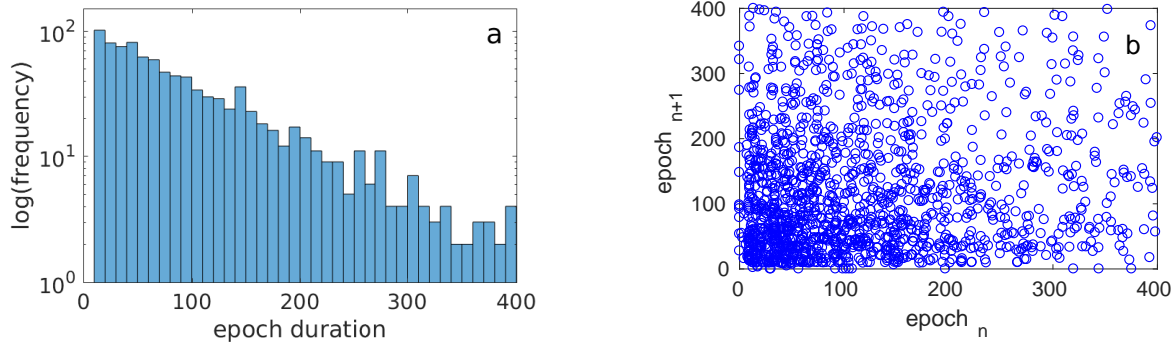


Figure 11: (a): Histogram of epoch durations smaller than 400, sorted into bins of width 10 years. The number of occurrences in each bin are displayed on a log scale to highlight the resemblance to an exponential frequency distribution. (b): Scatterplot of pairs of successive epoch durations smaller than 400.

decadal time scale. This is a stronger statement than saying that ENSO is chaotic. It places a time scale on the sensitive dependence on initial conditions. More specifically, our results show that epochs of relatively regular cycles of strong El Niño events like those observed during the past century might not continue. If they do cease, they may resume at any time.

We compare this unpredictability of ENSO regimes with ensemble weather forecasting. Ensemble forecasting is applied in situations where one expects sensitive dependence to initial conditions; i.e., nearby initial conditions yield trajectories that diverge from one another. This divergence happens gradually, so forecasting gives predictions with uncertainty that grows with time. Here, switching is abrupt and the time scale for predicting when a mode switch will take place seems to be comparable to the decadal time scale of strong El Niño events. Rapid divergence of nearby trajectories from one another is concentrated in small regions of the state space of the model. If we understand where this divergence takes place, then we can exploit that knowledge in our forecasts. We can also use what we have learned about the complex dynamics of the low dimensional JT model as a guide to gain deeper insight into the coupled oceanic and atmospheric dynamics of ENSO in large climate models. Whether the large scale dynamics of these large models have low dimensional attractors and almost invariant sets displaying different ENSO dynamics remain unanswered questions.

Acknowledgments: Henk Dijkstra’s work was partially supported by a Mary Shepard B. Upson Visiting Professor position at the College of Engineering of Cornell University, Ithaca, NY. He thanks for Prof. Paul Steen (Cornell University) for being his host and the many interesting discussions. Axel Timmermann was supported by the Institute for Basic Science (project code IBS-R028-D1).

References

- [1] Soon-Il An and Fei-Fei Jin. Nonlinearity and asymmetry of enso. *Journal of Climate*, 17(12):2399–2412, 2004.
- [2] Anthony G. Bamston, Muthuvel Chelliah, and Stanley B. Goldenberg. Documentation of a highly ENSO related SST region in the equatorial pacific: Research note. *Atmosphere-Ocean*, 35(3):367–383, 1997.
- [3] Michael Benedicks and Lai-Sang Young. Absolutely continuous invariant measures and random perturbations for certain one-dimensional maps. *Ergodic Theory Dynam. Systems*, 12(1):13–37, 1992.
- [4] K.M. Cobb, C. D. Charles, H. Cheng, and R. L. Edwards. El Niño-Southern Oscillation and tropical Pacific climate during the last millenium. *Nature*, 424:271–276, 2003.
- [5] Wellington de Melo and Sebastian van Strien. *One-dimensional dynamics*, volume 25 of *Ergebnisse der Mathematik und ihrer Grenzgebiete (3) [Results in Mathematics and Related Areas (3)]*. Springer-Verlag, Berlin, 1993.

- [6] Mathieu Desroches, John Guckenheimer, Bernd Krauskopf, Christian Kuehn, Hinke M. Osinga, and Martin Wechselberger. Mixed-mode oscillations with multiple time scales. *SIAM Rev.*, 54(2):211–288, 2012.
- [7] A. Dhooge, W. Govaerts, and Yu. A. Kuznetsov. MATCONT: a MATLAB package for numerical bifurcation analysis of ODEs. *ACM Trans. Math. Software*, 29(2):141–164, 2003.
- [8] W. Duan, X. Liu, K. Zhu, and M. Mu. Exploring the initial errors that casue a significant “spring predictability barrier” for El Niño events. *J. Geophys. Res.*, 114:C04022, 2009.
- [9] J.-P. Eckmann. Roads to turbulence in dissipative dynamical systems. *Rev. Modern Phys.*, 53(4, part 1):643–654, 1981.
- [10] Mark I. Freidlin and Alexander D. Wentzell. *Random perturbations of dynamical systems*, volume 260 of *Grundlehren der Mathematischen Wissenschaften [Fundamental Principles of Mathematical Sciences]*. Springer, Heidelberg, third edition, 2012. Translated from the 1979 Russian original by Joseph Szücs.
- [11] Gary Froyland and Michael Dellnitz. Detecting and locating near-optimal almost-invariant sets and cycles. *SIAM J. Sci. Comput.*, 24(6):1839–1863, 2003.
- [12] Celso Grebogi, Edward Ott, and James A. Yorke. Crises, sudden changes in chaotic attractors, and transient chaos. *Phys. D*, 7(1-3):181–200, 1983. Order in chaos (Los Alamos, N.M., 1982).
- [13] Celso Grebogi, Edward Ott, and James A. Yorke. Chaos, strange attractors, and fractal basin boundaries in nonlinear dynamics. *Science*, 238(4827):632–638, 1987.
- [14] John Guckenheimer and Philip Holmes. *Nonlinear oscillations, dynamical systems, and bifurcations of vector fields*, volume 42 of *Applied Mathematical Sciences*. Springer-Verlag, New York, 1990. Revised and corrected reprint of the 1983 original.
- [15] G. Haller. Distinguished material surfaces and coherent structures in three-dimensional fluid flows. *Phys. D*, 149(4):248–277, 2001.
- [16] FF Jin. An equatorial ocean recharge paradigm for ENSO .1. Conceptual model. *J. Atmos. Sci.*, 54(7):811–829, APR 1 1997.
- [17] M. T. M. Koper and P. Gaspard. The modeling of mixed-mode and chaotic oscillations in electrochemical systems. *J. Chem. Phys.*, 96(10):7797–7813, 1992.
- [18] M. Latif, T. P. Barnett, M. A. Cane, M. Flügel, N. E. Graham, H. von Storch, J.-S. Xu, and S. E. Zebiak. A review of ENSO prediction studies. *Clim. Dynam.*, 9:167–179, 1994.
- [19] S. McGregor, A. Timmermann, M. H. England, O. Elison Timm, and A. T. Wittenberg. Inferred changes in El Nino-Southern Oscillation variance over the past six centuries. *Climate of the Past*, 9(5):2269–2284, 2013.
- [20] Michael J McPhaden, Axel Timmermann, Matthew J Widlansky, Magdalena A Balmaseda, and Timothy N Stockdale. The Curious Case of the EL Niño That Never Happened: A Perspective from 40 Years of Progress in Climate Research and Forecasting. *Bull. Amer. Meteor. Soc.*, 96(10):1647–1665, October 2015.
- [21] M. Mu, W. Duan, and B. Wang. Season-dependent dynamics of nonlinear optimal error growth and ENSO predictability in a theoretical model. *J. Geophys. Res.*, 112:D10113, 2007.
- [22] Andrew Roberts, John Guckenheimer, Esther Widiasih, Axel Timmermann, and Christopher K. R. T. Jones. Mixed-Mode Oscillations of El Niño–Southern Oscillation. *J. Atmos. Sci.*, 73(4):1755–1766, 2016.
- [23] David Ruelle. Sensitive dependence on initial condition and turbulent behavior of dynamical systems. In *Bifurcation theory and applications in scientific disciplines (Papers, Conf., New York, 1977)*, volume 316 of *Ann. New York Acad. Sci.*, pages 408–416. New York Acad. Sci., New York, 1979.

- [24] Marten Scheffer. *Critical Transitions in Nature and Society: (Princeton Studies in Complexity)*. Princeton University Press, 2009.
- [25] MJ Suarez and PS Schopf. A delayed action model for ENSO. *J. Atmos. Sci.*, 45(21):3283–3287, NOV 1 1988.
- [26] Axel Timmermann and Fei-Fei Jin. Predictability of coupled processes. *Predictability of weather and climate*, pages 251–274, 2006.
- [27] Axel Timmermann, Fei-Fei Jin, and Jan Abshagen. A nonlinear theory for El Niño bursting. *J. Atmos. Sci.*, 60(1):152–165, 2003.
- [28] E Tziperman, MA Cane, SE Zebiak, Y Xue, and B Blumenthal. Locking of El Niño’s peak time to the end of the calendar year in the delayed oscillator picture of ENSO. *J. Climate*, 11(9):2191–2199, SEP 1998.
- [29] P. J. Webster. The annual cycle and the predictability of the tropical coupled ocean-atmosphere system. *Meteor. Atmos. Phys.*, 56:33–55, 1995.
- [30] PJ Webster and S Yang. Monsoon and ENSO: Selectively interactive systems. *Q. J. R. Meteor. Soc.*, 118:877–926, 1992.
- [31] Andrew T. Wittenberg. Are historical records sufficient to constrain ENSO simulations? *Geophysical Research Letters*, 36(12):n/a–n/a, 2009. L12702.
- [32] Andrew T. Wittenberg, Anthony Rosati, Thomas L. Delworth, Gabriel A. Vecchi, and Fanrong Zeng. ENSO Modulation: Is It Decadally Predictable? *Journal of Climate*, 27(7):2667–2681, 2014.
- [33] Lai-Sang Young. Ergodic theory of attractors. In *Proceedings of the International Congress of Mathematicians, Vol. 1, 2 (Zürich, 1994)*, pages 1230–1237. Birkhäuser, Basel, 1995.
- [34] Y. Yu, M. Mu, and W. Duan. Does model parameter error cause a significant spring predictability barrier for El Niño events in the Zebiak-Cane model. *J. Climate*, 25:1263–1277, 2012.